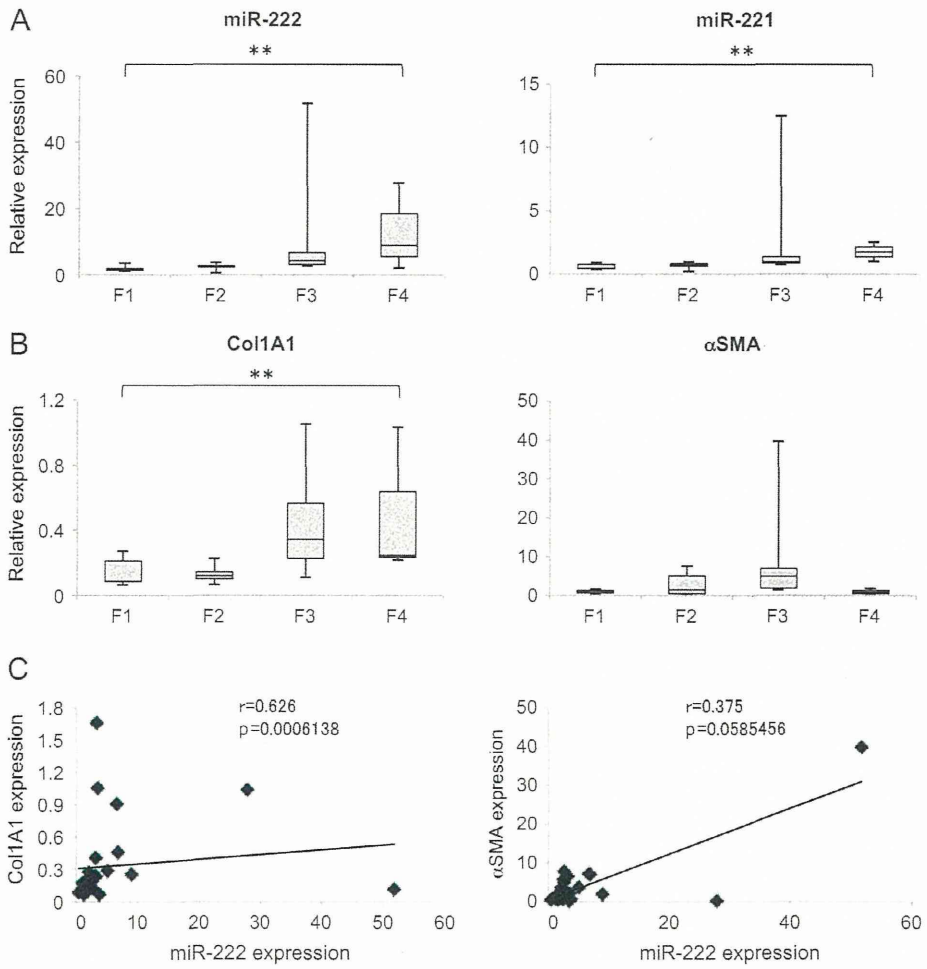

Figure 3 Levels of microRNA (miRNA)-221/222 and their correlation with Col1A1 and α-smooth muscle actin (αSMA) mRNA levels in patients with non-alcoholic steatohepatitis (NASH). (A) Expression of miR-221/222 in 26 patients with NASH. The expression levels are indicated relative to F1. The Jonckheere–Terpstra test for ordered alternatives was used to identify trends among classes. **p<0.01. (B) Expression of Col1A1 and αSMA mRNAs in 26 patients with NASH. The expression levels are indicated relative to F1. Glyceraldehyde 3-phosphate dehydrogenase was used as an internal control. The Jonckheere–Terpstra test for ordered alternatives was used to identify trends among classes. **p<0.01. (C) Correlation between miR-222 expression and Col1A1 or αSMA mRNA expression. Correlation coefficients between parameters were evaluated by Spearman rank correlations.

miR-222 transcription is regulated by NF-κB; the genomic region upstream of human miR-222 has multiple NF-κB binding elements.[33] NF-κB regulates Col1A1 gene expression and stellate cell activation.[34–36] Thus, we studied whether NF-κB stimulators, such as TGFα and TNFα, induce miR-222 expression and, in contrast, whether an NF-κB inhibitor (QNZ) inhibits its expression. As shown in figure 5D, stimulation of stellate cells with TGFα (1 or 10 ng/ml) or TNFα (0.1 or 1 ng/ml) for 24 h from day 1 to day 2 upregulated miR-222 expression, while QNZ (10 or 100 nmol/l) significantly reduced it. Stimulation of stellate cells with TGFα (1 ng/ml) or TNFα (0.1 ng/ml) for 72 h from day 1 to day 4 upregulated miR-222 expression by 1.9-fold (p<0.01) or 1.3-fold (p<0.05), respectively, compared with the untreated control (figure 5E) and miR-222 upregulation was inhibited to 18% or 26% of the untreated control level, respectively, by QNZ (figure 5E). These results indicate that miR-222 expression in stellate cells is regulated by NF-κB activation. QNZ (10 nmol/l) inhibited the activation-associated morphological transition of mouse hepatic stellate cells (figure 5F). This condition attenuated the expression of Col1A1 mRNA to 21% (p<0.01) and αSMA mRNA to 63% (p<0.01) of the untreated control levels (figure 5G).

Interaction of miR-222 with the *CDKN1B* 3′UTR in human stellate cells

miR-221 controls CDKN1B and CDKN1C expression in HCC cell lines.[37] The prediction of miRNA target regions by TargetScan (http://www.targetscan.org/) indicated that the *CDKN1B* 3′UTR has two target regions for miR-221/222 (figure 6A). Here, we investigated the presence of a direct interaction between miR-222 and CDKN1B mRNA in LX-2 cells by the firefly luciferase reporter assay and found that the miR-222 precursors inhibited luciferase activity derived from vectors carrying the *CDKN1B* 3′UTR (figure 6B). These observations indicate that the *CDKN1B* 3′UTR could be targeted by miR-222 in LX-2 cells.

Next, we transfected miR-222 precursors and miR-222 inhibitors into LX-2 cells. The transient transfection of miR-222 precursors significantly inhibited CDKN1B mRNA and protein expression compared with their expression in cells transfected with the negative control miRNA (figure 6C). Additionally, the transfection of miR-222 inhibitors significantly upregulated CDKN1B mRNA and protein expression in comparison with cells transfected with the negative control miRNA (figure 6D). Even though the transfection of miR-222 precursors or inhibitors into LX-2 cells showed negligible effects on cell growth (figure 6E,F), these results indicate that miR-222 targets *CDKN1B* in LX-2 cells.

Additional analyses indicated that transient transfection with miR-222 precursors significantly upregulated Col1A1 and matrix metalloproteinase 2 (MMP-2) mRNA expression and downregulated MMP-1, MMP-9 and TGFβ1 mRNA expression via unknown mechanisms (figure 6G).

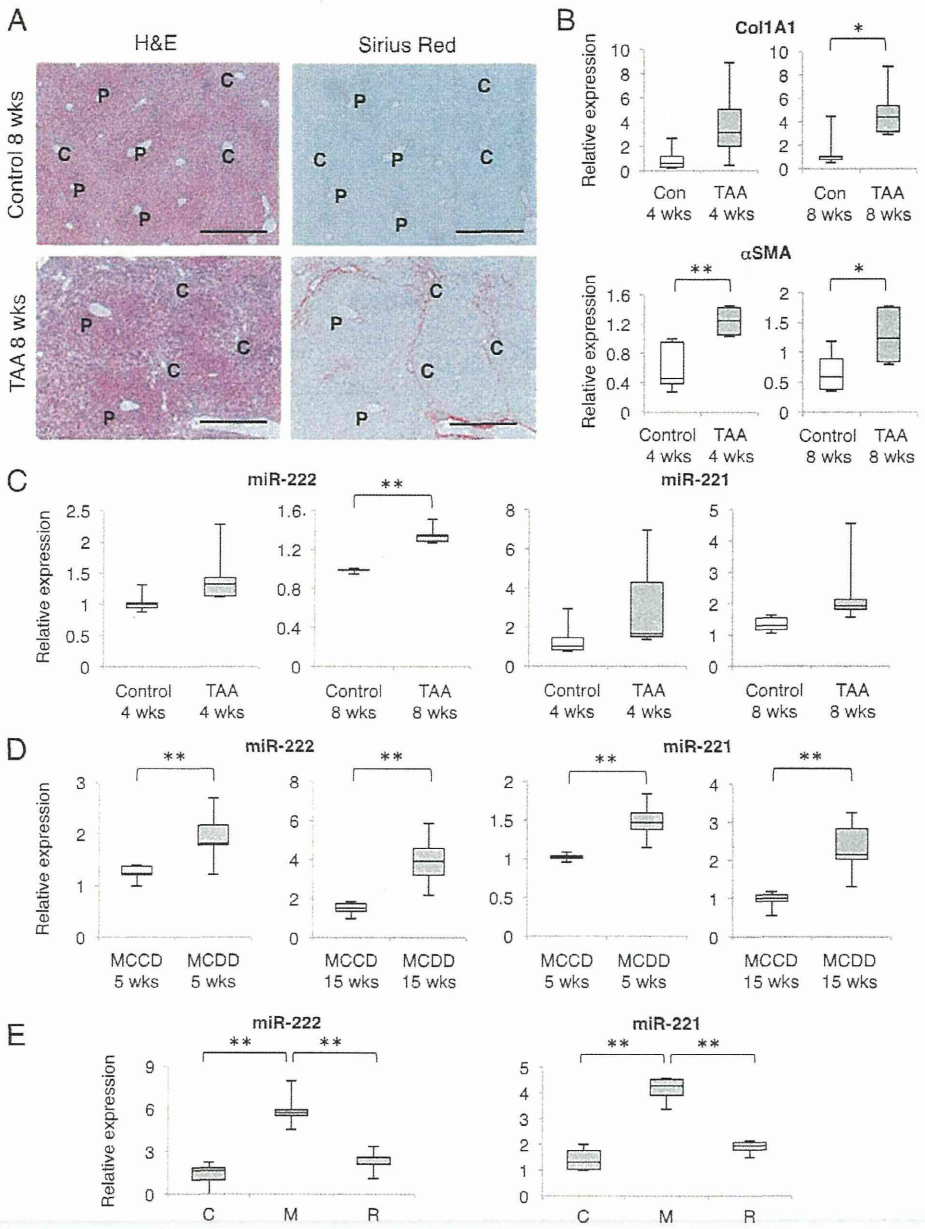

Figure 4 Expression of miR-221/222 in mouse models of liver fibrosis. (A) Liver fibrosis was induced in mice by injecting 200 μg/g body weight of thioacetamide (TAA) for 8 weeks. Haematoxylin and eosin staining (H&E; left). Sirius red staining (right). Scale bars, 200 μm. C, central vein area; P, portal vein area. (B) mRNA expression of Col1A1 and α-smooth muscle actin (αSMA) in TAA-induced liver fibrosis. The expression levels are indicated relative to control livers. Glyceraldehyde 3-phosphate dehydrogenase was used as an internal control. *p<0.05, **p<0.01 compared with control. (C) Expression of miR-221 and miR-222 in TAA-induced liver fibrosis. The expression levels are indicated relative to control livers. **p<0.01 compared with control. In B and C, open columns indicate data from controls and closed columns from TAA. (D) Expression of miR-221 and miR-222 in a methionine- and choline-deficient diet (MCDD)-induced liver fibrosis. The expression levels are indicated relative to methionine-choline control diet (MCCD) mouse livers. **p<0.01 compared with MCCD. Open columns indicate data from MCCD and closed columns from MCDD. (E) Expression of miR-221 and miR-222 in MCDD-induced liver fibrosis in rats.[27] The expression levels are indicated relative to rats fed MCCD for 10 weeks (C). Liver miR-221 and miR-222 levels significantly decreased in the recovery phase (R, MCDD for 8 weeks followed by MCCD for 2 weeks) compared with those fed MCDD for 10 weeks (M). **p<0.01.

DISCUSSION

Our study explored miRNA expression profiles during the progression of liver fibrosis in patients infected with HCV using microarray analysis. The expression of miR-222 was significantly correlated with that of Col1A1 and αSMA mRNAs in patients with HCV and with the expression of miR-221. To our knowledge, this is the first report to identify miR-221 and miR-221 as fibrosis-related molecules and to report miR-221/222 expression in a liver pathology other than carcinogenesis. Our results additionally indicate the close correlation between miR-221/222 and Col1A1 mRNA expression in the livers of people with NASH.

Recently, Roderburg *et al* reported the upregulation of miR-125-5p, miR-199b-3p, miR-221 and miR-302 and the downregulation of miR-29 family members in CCl_4-treated mouse livers, as observed using microarray analysis and quantitative RT-PCR.[38] Murakami *et al* reported that increased miR-199a-5p, miR-199a-3p, miR-200a and miR-200b levels are significantly associated with the progression of liver fibrosis in both humans and mice and that the overexpression of miR-199a-3p in human stellate cells results in the significant induction of tissue inhibitor of MMP-1, Col1A1 and MMP-13.[32] Furthermore, the expression levels of miR-21 and miR-122 have been correlated with the histological findings of HCV-induced liver disease.[23] However, in our analyses, although the expression of miR-199a-5p, miR-199a-3p and miR-21 tended to increase in activated mouse stellate cells during culture (0.8- and 2.1-fold for miR-199a-5p, 0.7- and 1.5-fold for miR-199a-3p and 1.9- and 3.8-fold for miR-21 at day 4 and day 7, respectively, compared with day 1), they failed to increase more than 10-fold, as miR-221 and miR-222 did (data not shown). Thus, miR-222 and miR-221 are more likely to reflect the activation of stellate cells than miR-199a-5p, miR-199a-3p and miR-21, similarly to the expression of Col1A1 mRNA.

It is generally accepted that liver fibrosis is a major risk factor for the development of HCC. A national surveillance

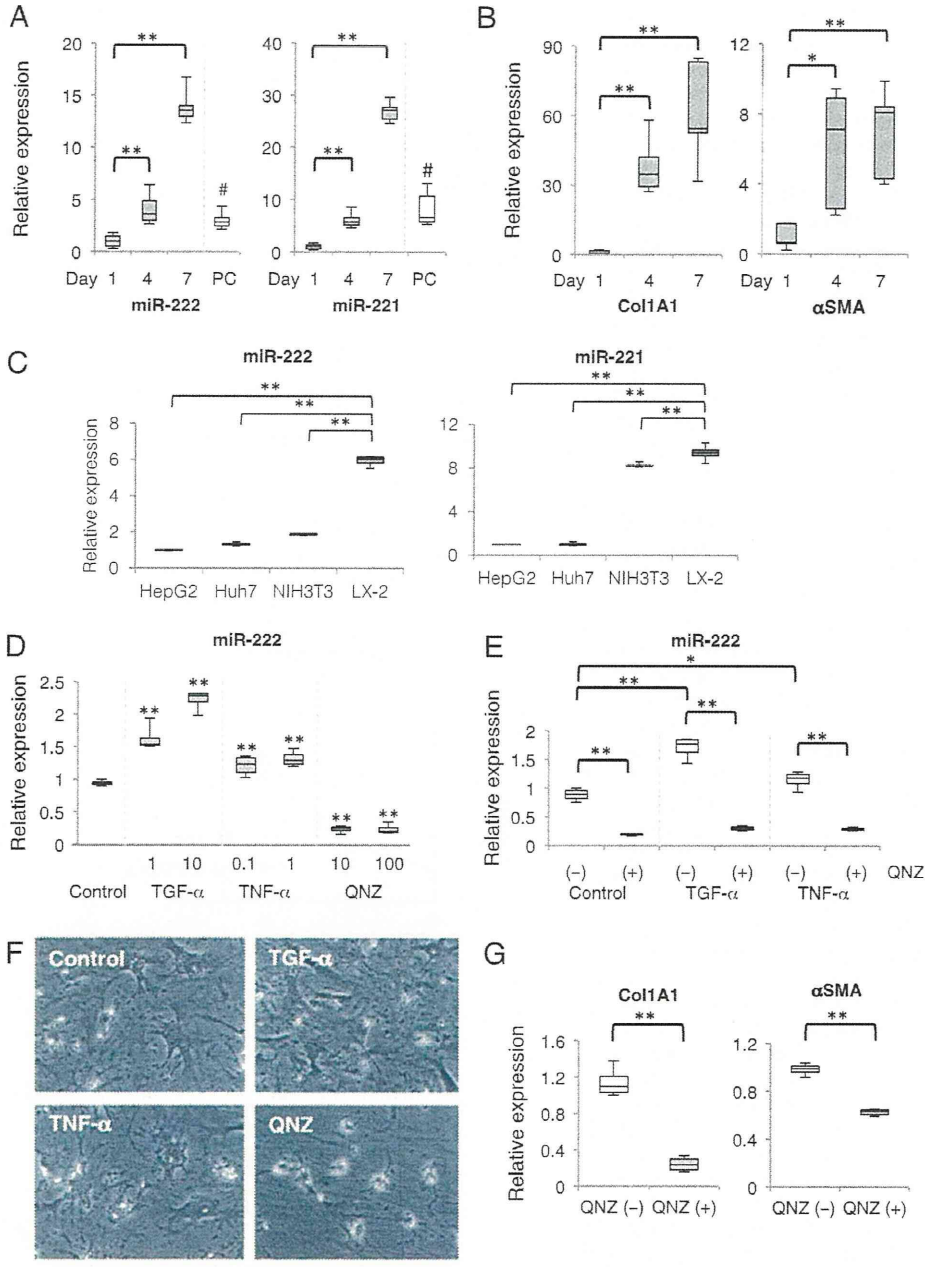

Figure 5 Regulation of miR-222 expression in stellate cells. (A) Expression of miR-221 and miR-222 in mouse stellate cells during primary culture. Isolated mouse stellate cells were cultured for the indicated periods. **p<0.01. PC indicates the expression of miR-221 and miR-222 in isolated mouse hepatocytes. #p<0.01 compared with stellate cells at day 7. (B) Expression of Col1A1 and α-smooth muscle actin (αSMA) mRNAs in mouse stellate cells during primary culture. Glyceraldehyde 3-phosphate dehydrogenase was used as an internal control. *p<0.05, **p<0.01. (C) Expression of miR-221 and miR-221 in HepG2, Huh7, NIH3T3 and LX-2. **p<0.01. (D and E) Regulation of miR-222 expression in mouse primary stellate cells. D: At 1 day after culture, the cells were treated with transforming growth factor α (TGFα; 1 or 10 ng/ml), tumour necrosis factor α (TNFα; 0.1 or 1 ng/ml), or 6-amino-4-(4-phenoxyphenylethylamono) quinazoline (QNZ; 10 or 100 nmol/l) for 24 h. Control indicates non-treated cells. **p<0.01 compared with control. E: At 1 day after culture, the cells were treated with TGFα (1 ng/ml), TNFα (0.1 ng/ml), QNZ (10 nmol/l), TGFα (1 ng/ml) plus QNZ (10 nmol/l), or TNFα (0.1 ng/ml) plus QNZ (10 nmol/l) for 72 h. Control indicates non-treated cells. *p<0.05, **p<0.01. (F) Morphology of mouse stellate cells observed under a microscope (×200) as in (E). (G) Expression of Col1A1 and αSMA mRNAs in mouse stellate cells treated with or without QNZ (10 nmol/l) during primary culture for 72 h.

programme in Japan has estimated that the annual incidence of HCC is 0.5–2.0% (mild liver fibrosis; F1/F2) and 5.3–7.9% (advanced liver fibrosis; (F3/F4) among patients with chronic hepatitis C.[39] miR-221 and miR-222, a pair of miRNAs encoded in a cluster on chromosome X, are overexpressed in a variety of human cancers, including HCC, in which they play oncogenic roles by downregulating p27, p57 and PTEN expression.[22 37 40] In particular, the pro-tumour activity of miR-221/222 is thought to be achieved by its regulation of CDKN1B (p27, Kip1).[41 42] In this study, we showed that miR-222 interacts with the *CDKN1B* 3′UTR and inhibits the expression of CDKN1B mRNA and protein in LX-2 cells, although it is unclear why increased miR-222 fails to affect the proliferation of stellate cells (figure 6). Type I interferon inhibits the proliferation of LX-2 cells by decreasing cyclin E and increasing p21 without affecting the expression of CDKN1B (p27).[31] In this regard, the proliferation of stellate cells may be strongly regulated by p21 rather than p27.

In general, miRNAs are transcribed by RNA polymerase II as part of capped and polyadenylated primary transcripts. The primary transcript is cleaved by the Drosha ribonuclease III to generate an approximately 70-nt stem-loop precursor miRNA, which is further cleaved by the cytoplasmic Dicer ribonuclease to generate the mature miRNA. In addition to this common pathway, recent investigations have shown that other factors are involved in the transcription of miRNAs by binding to their promoter regions. For instance, Galardi *et al* identified two separate regions upstream of the miR-221/222 promoter that are bound by the NF-κB subunit p65 and drive efficient transcription in luciferase reporter assays, indicating that the expression of miR-221/222 is induced by NF-κB activation in prostate carcinoma and glioblastoma cells.[33] Because NF-κB is involved in

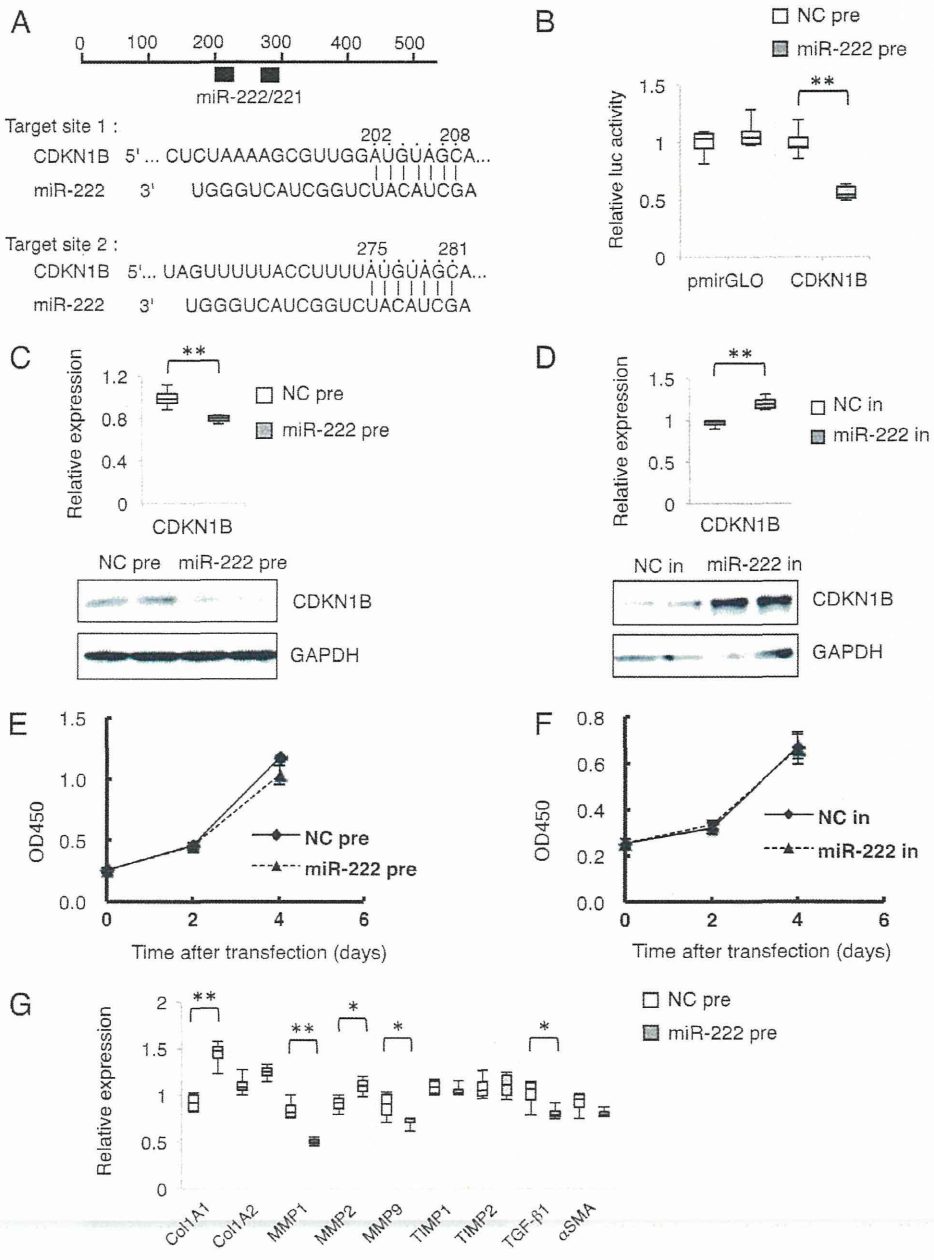

Figure 6 Interaction of miR-222 with the 3′UTR of CDKN1B mRNA. (A) Schematic indication of the miR-221/222 binding sites in the 3′UTR of CDKN1B mRNA based on TargetScan Human Release 5.1 (http://www.targetscan.org/). Black boxes indicate miR-221 or miR-222. Two predicted target sites of miR-221/222 are present in the 3′UTR of CDKN1B mRNA. (B) Reporter gene assay to test the interaction between the 3′UTR of CDKN1B mRNA and miR-222 in LX-2 cells. Relative luciferase activity derived from pCDKN1B–miR-222/mirGLO in the presence of miR-222 precursors. The pmirGLO vector was used as a negative control reporter vector. NC pre: co-transfection of reporter vectors together with a negative control miRNA precursor, which has a scrambled sequence. miR-222 pre: co-transfection of reporter vectors together with miR-222 precursors. The results are expressed relative to the activity in the presence of negative control precursors. **p<0.01. (C) Effect of miR-222 precursors on the expression of CDKN1B mRNA and protein in LX-2 cells. LX-2 cells were transfected with 50 nM miR-222 precursor (grey column) or a negative control (white column). At 24 h after transfection, CDKN1B mRNA (upper) and protein (lower) were measured. Glyceraldehyde 3-phosphate dehydrogenase (GAPDH) was used as an internal control. **p<0.01. (D) Effect of miR-222 inhibitors on the expression of CDKN1B mRNA and protein in LX-2 cells. LX-2 cells were transfected with 50 nM miR-222 inhibitor (grey column) or a negative control (white column). At 24 h after transfection, CDKN1B mRNA (upper) and protein (lower) were measured. GAPDH was used as an internal control. **p<0.01. (E, F) Effect of 50 nM miR-222 precursors (E) and inhibitors (F) on LX-2 cell growth, determined by WST-1 assay. (G) Effect of miR-222 precursors on the expression of fibrosis-related mRNAs in LX-2 cells. LX-2 cells were transfected with 50 nM miR-222 precursor (grey column) or a negative control (white column). At 24 h after transfection, the mRNAs were quantified. GAPDH was used as an internal control. *p<0.05, **p<0.01. ColA1, α1 (I) collagen; MMP, matrix metalloproteinase; αSMA, α-smooth muscle actin; TGFβ1, transforming growth factor β1; TIMP, tissue inhibitor of matrix metalloproteinase.

the process of stellate cell activation,[34–36] we speculated that the expression of miR-222 might be regulated through NF-κB activation in stellate cells. We found, however, that miR-222 expression was inhibited by QNZ, an NF-κB inhibitor, accompanied by the morphological maintenance of quiescence, and upregulated by the NF-κB activators TNFα and TGFα.

miRNA expression profiles can serve as useful tools for understanding and investigating the mechanism of the progression of liver fibrosis and can serve as new fibrosis biomarkers. miRNAs are packed into exosomes and circulate in blood.[43] However, this raises the question of whether circulating levels of miRNAs in blood correlate with the progression of liver fibrosis at the tissue level. Roderburg *et al* demonstrated that the expression levels of miR-29 family members in human liver fibrosis correlate with the downregulation of miR-29a in the serum.[38] Here, we observed that the expression of miR-222 in human livers with chronic trauma significantly correlated with the expression of Col1A1 mRNA, suggesting that miR-222 is a potential biomarker of liver fibrosis progression, although its utility as a serum biomarker needs further validation. Li *et al* recently reported that the miR-221 level in blood correlates with cirrhosis, tumour size and tumour stage and provides predictive value for prognosis in patients with HCC.[44]

This study has some limitations. The molecular mechanisms of liver fibrosis in viral hepatitis and in NASH may not exactly the same. In addition, fibrosis in human livers usually progresses

slowly, over the course of decades, so it is not practical to examine the expression of miRNAs at time points throughout progression. In contrast, liver fibrosis in experimental animals progresses quickly, so that within several weeks we could track the changes in miRNA expression at several time points. To establish the utility of miR-221/222 as biomarkers of liver fibrosis irrespective of aetiology, further studies are required to understand the exact mechanism by which the miRNAs participate in the progression of fibrosis.

In conclusion, we showed that miR-221 and miR-222 may be new markers for stellate cell activation and liver fibrosis progression in both humans and mice. These miRNAs could be used in the diagnosis of human liver fibrosis in clinical practice in the near future.

Acknowledgements We thank Drs Hiroyuki Motoyama, Le Thi Thanh Thuy, Masashi Iizuka and Tohru Komiya; Miss Shinobu Momen and Mrs Mami Mori for their valuable comments on this study.

Funding NK was supported by a grant-in-aid for scientific research from the Japan Society for the Promotion of Science (JSPS) (No 21390232; 2009—2011), a grant from the Ministry of Health, Labour and Welfare of Japan (2008—2010) and a Thrust Area Research Grant from Osaka City University (2008—2011). TO was supported by a grant-in-aid for scientific research from the JSPS (No 22790666; 2010—2011).

Competing interests None.

Ethics approval Ethics approval was provided by Osaka City University Medical School.

Contributors TO, EM, NK: conception, design, analysis and interpretation of data, drafting of the manuscript, critical revision of article, final approval given. HF, YS: analysis and interpretation of data, final approval given. KY, KI: conception, design, drafting of the manuscript, final approval given.

Provenance and peer review Not commissioned; externally peer reviewed.

REFERENCES

1. **Friedman SL.** Evolving challenges in hepatic fibrosis. *Nat Rev Gastroenterol Hepatol* 2010;**7**:425—36.
2. **Angulo P.** Nonalcoholic fatty liver disease. *N Engl J Med* 2002;**346**:1221—31.
3. **Matteoni CA,** Younossi ZM, Gramlich T, *et al.* Nonalcoholic fatty liver disease: a spectrum of clinical and pathological severity. *Gastroenterology* 1999;**116**:1413—19.
4. **Brunt EM,** Janney CG, Di Bisceglie AM, *et al.* Nonalcoholic steatohepatitis: a proposal for grading and staging the histological lesions. *Am J Gastroenterol* 1999;**94**:2467—74.
5. **Friedman SL.** Molecular regulation of hepatic fibrosis, an integrated cellular response to tissue injury. *J Biol Chem* 2000;**275**:2247—50.
6. **Kawada N.** Evolution of hepatic fibrosis research. *Hepatol Res* 2011;**41**:199—208.
7. **Wake K.** "Sternzellen" in the liver: perisinusoidal cells with special reference to storage of vitamin A. *Am J Anat* 1971;**132**:429—62.
8. **Filipowicz W,** Bhattacharyya SN, Sonenberg N. Mechanisms of post-transcriptional regulation by microRNAs: are the answers in sight? *Nat Rev Genet* 2008;**9**:102—14.
9. **Bartel DP.** MicroRNAs: genomics, biogenesis, mechanism and function. *Cell* 2004;**116**:281—97.
10. **Brennecke J,** Hipfner DR, Stark A, *et al.* bantam encodes a developmentally regulated microRNA that controls cell proliferation and regulates the proapoptotic gene hid in Drosophila. *Cell* 2003;**113**:25—36.
11. **Schratt GM,** Tuebing F, Nigh EA, *et al.* A brain-specific microRNA regulates dendritic spine development. *Nature* 2006;**439**:283—9.
12. **Chen CZ,** Li L, Lodish HF, *et al.* MicroRNAs modulate hematopoietic lineage differentiation. *Science* 2004;**303**:83—6.
13. **Kota J,** Chivukula RR, O'Donnell KA, *et al.* Therapeutic microRNA delivery suppresses tumorigenesis in a murine liver cancer model. *Cell* 2009;**137**:1005—17.
14. **Chen JF,** Murchison EP, Tang R, *et al.* Targeted deletion of Dicer in the heart leads to dilated cardiomyopathy and heart failure. *Proc Natl Acad Sci U S A* 2008;**105**:2111—16.
15. **Perkins DO,** Jeffries CD, Jarskog LF, *et al.* microRNA expression in the prefrontal cortex of individuals with schizophrenia and schizoaffective disorder. *Genome Biol* 2007;**8**:R27.
16. **Lewis AP,** Jopling CL. Regulation and biological function of the liver-specific miR-122. *Biochem Soc Trans* 2010;**38**:1553—7.
17. **Jopling CL,** Yi M, Lancaster AM, *et al.* Modulation of hepatitis C virus RNA abundance by a liver-specific MicroRNA. *Science* 2005;**309**:1577—81.
18. **Li YP,** Gottwein JM, Scheel TK, *et al.* MicroRNA-122 antagonism against hepatitis C virus genotypes 1-6 and reduced efficacy by host RNA insertion or mutations in the HCV 5' UTR. *Proc Natl Acad Sci U S A* 2011;**108**:4991—6.
19. **Lanford RE,** Hildebrandt-Eriksen ES, Petri A, *et al.* Therapeutic silencing of microRNA-122 in primates with chronic hepatitis C virus infection. *Science* 2010;**327**:198—201.
20. **Pedersen IM,** Cheng G, Wieland S, *et al.* Interferon modulation of cellular microRNAs as an antiviral mechanism. *Nature* 2007;**449**:919—22.
21. **Sarasin-Filipowicz M,** Krol J, Markiewicz I, *et al.* Decreased levels of microRNA miR-122 in individuals with hepatitis C responding poorly to interferon therapy. *Nat Med* 2009;**15**:31—3.
22. **Pineau P,** Volinia S, McJunkin K, *et al.* miR-221 overexpression contributes to liver tumorigenesis. *Proc Natl Acad Sci U S A* 2010;**107**:264—9.
23. **Marquez RT,** Bandyopadhyay S, Wendlandt EB, *et al.* Correlation between microRNA expression levels and clinical parameters associated with chronic hepatitis C viral infection in humans. *Lab Invest* 2010;**90**:1727—36.
24. **Bedossa P,** Poynard T. An algorithm for the grading of activity in chronic hepatitis C. The METAVIR Cooperative Study Group. *Hepatology* 1996;**24**:289—93.
25. **Sato F,** Tsuchiya S, Terasawa K, *et al.* Intra-platform repeatability and inter-platform comparability of microRNA microarray technology. *PLoS One* 2009;**4**:e5540.
26. **Ikejima K,** Honda H, Yoshikawa M, *et al.* Leptin augments inflammatory and profibrogenic responses in the murine liver induced by hepatotoxic chemicals. *Hepatology* 2001;**34**:288—97.
27. **Mu YP,** Ogawa T, Kawada N. Reversibility of fibrosis, inflammation and endoplasmic reticulum stress in the liver of rats fed a methionine-choline-deficient diet. *Lab Invest* 2010;**90**:245—56.
28. **Kristensen DB,** Kawada N, Imamura K, *et al.* Proteome analysis of rat hepatic stellate cells. *Hepatology* 2000;**32**:268—77.
29. **Xu L,** Hui AY, Albanis E, *et al.* Human hepatic stellate cell lines, LX-1 and LX-2: new tools for analysis of hepatic fibrosis. *Gut* 2005;**54**:142—51.
30. **Ogawa T,** Iizuka M, Sekiya Y, *et al.* Suppression of type I collagen production by microRNA-29b in cultured human stellate cells. *Biochem Biophys Res Commun* 2010;**391**:316—21.
31. **Sekiya Y,** Ogawa T, Iizuka M, *et al.* Down-regulation of cyclin E1 expression by microRNA-195 accounts for interferon-beta-induced inhibition of hepatic stellate cell proliferation. *J Cell Physiol* 2011;**226**:2535—42.
32. **Murakami Y,** Toyoda H, Tanaka M, *et al.* The progression of liver fibrosis is related with overexpression of the miR-199 and 200 families. *PLoS One* 2011;**6**:e16081.
33. **Galardi S,** Mercatelli N, Farace MG, *et al.* NF-kB and c-Jun induce the expression of the oncogenic miR-221 and miR-222 in prostate carcinoma and glioblastoma cells. *Nucleic Acids Res* 2011;**39**:3892—902.
34. **Lee KS,** Buck M, Houglum K, *et al.* Activation of hepatic stellate cells by TGF alpha and collagen type I is mediated by oxidative stress through c-myb expression. *J Clin Invest* 1995;**96**:2461—8.
35. **Rippe RA,** Schrum LW, Stefanovic B, *et al.* NF-kappaB inhibits expression of the alpha1(I) collagen gene. *DNA Cell Biol* 1999;**18**:751—61.
36. **Lang A,** Schoonhoven R, Tuvia S, *et al.* Nuclear factor kappaB in proliferation, activation and apoptosis in rat hepatic stellate cells. *J Hepatol* 2000;**33**:49—58.
37. **Fornari F,** Gramantieri L, Ferracin M, *et al.* MiR-221 controls CDKN1C/p57 and CDKN1B/p27 expression in human hepatocellular carcinoma. *Oncogene* 2008;**27**:5651—61.
38. **Roderburg C,** Urban GW, Bettermann K, *et al.* Micro-RNA profiling reveals a role for miR-29 in human and murine liver fibrosis. *Hepatology* 2011;**53**:209—18.
39. **Yoshida H,** Shiratori Y, Moriyama M, *et al.* Interferon therapy reduces the risk for hepatocellular carcinoma: national surveillance program of cirrhotic and noncirrhotic patients with chronic hepatitis C in Japan. IHIT Study Group. Inhibition of Hepatocarcinogenesis by Interferon Therapy. *Ann Intern Med* 1999;**131**:174—81.
40. **Garofalo M,** Di Leva G, Romano G, *et al.* miR-221&222 regulate TRAIL resistance and enhance tumorigenicity through PTEN and TIMP3 downregulation. *Cancer Cell* 2009;**16**:498—509.
41. **le Sage C,** Nagel R, Egan DA, *et al.* Regulation of the p27(Kip1) tumor suppressor by miR-221 and miR-222 promotes cancer cell proliferation. *Embo J* 2007;**26**:3699—708.
42. **Galardi S,** Mercatelli N, Giorda E, *et al.* miR-221 and miR-222 expression affects the proliferation potential of human prostate carcinoma cell lines by targeting p27Kip1. *J Biol Chem* 2007;**282**:23716—24.
43. **Kosaka N,** Iguchi H, Ochiya T. Circulating microRNA in body fluid: a new potential biomarker for cancer diagnosis and prognosis. *Cancer Sci* 2010;**101**:2087—92.
44. **Li J,** Wang Y, Yu W, *et al.* Expression of serum miR-221 in human hepatocellular carcinoma and its prognostic significance. *Biochem Biophys Res Commun* 2011;**406**:70—3.

Mice with Liver Composed of Human Hepatocytes as an Animal Model for Drug Testing

Katsutoshi Yoshizato[1,2,*], Chise Tateno[1], and Rie Utoh[3]

[1]*Phoenixbio Co., Ltd, Hiroshima, Japan;* [2]*Liver Research Center and Synthetic Biology Laboratory, Osaka City University Graduate School of Medicine, Osaka, Japan and* [3]*The Institute of Advanced Biomedical Engineering and Science, Tokyo Women's Medical University, Tokyo, Japan*

Abstract: Conventionally, rodents, mostly mice and rats, have been utilized as animal models for studying drug metabolism and toxicity of new medicines. However, there have been two major problems inherent to these models. One is that there are species differences in major enzymes responsible for drug metabolisms and detoxification such as cytochrome P450 between rodents and humans, and the other is that human hepatitis viruses do not infect rodent livers, which hampers studies for anti-hepatitis virus drugs using these models. As an approach to overcome these intrinsic shortages, we devised a method to generate mice whose livers are mostly (>80%) repopulated with healthy human hepatocytes 7 years ago. Since then, these mice called simply chimeric mice or liver-humanized mice have been widely utilized among researchers in the areas for new drug developments, which, as a result, have proved that the chimeric mouse is a practical solution to solve the above two issues. The hitherto accumulated studies demonstrating the similarities of the chimeric mouse liver to the human crude liver are summarized and reviewed in the present article. In addition, there have been also studies that show us the presence of dissimilarities between them, such as human hepatocytes' manifestation of hyperplasia in mouse liver and their steatotic alterations when the mice are maintained for >50 days post-transplantation. These dissimilarities between them are also reviewed in details, considering that the information of the similarities and the dissimilarities is quite useful to researchers who utilize chimeric mice as a drug discovery tool for correctly evaluating the obtained results.

Keyword: Growth hormone, hepatic stellate cells, hepatitis viruses, *in vivo* drug testing, liver regeneration, liver steatosis, Mice with human liver, TGF-β signaling.

INTRODUCTION

Science is the activity to understand a phenomenon of interest by knowing the relationships among the components that are included in a phenomenon. Usually, we are able to directly collect samples from entities that participate in a phenomenon and analyze the samples. However, samples from humans are generally hard to be collected even in the case of diseased persons, *i.e.* normal and healthy human samples are practically inaccessible except the cases in which test samples are considered to be indispensable to cure diseases. Rare healthy samples collected under exceptionally acceptable conditions are thus highly precious for revealing the biological and physiological features of human tissues and cells. As a matter of fact *in vivo* experimentation with humans to understand their normal processes of biological and physiological phenomena is impossible, contrasting with relative easiness of non-human vertebrates and free accessibility of non-vertebrates for the scientific purposes.

Conventionally, rodents, especially mice and rats, have been utilized as animal models for studies that aim to understand human biology and pathology in spite of the presence of species differences in many aspects of biological features between humans and rodents. Under these situations one possible approach for revealing *in vivo* features of human tissues and cells has been to create a rodent that bears human tissues/cells. A major target organ for studying drug metabolism and toxicity in R&D areas of new medicines is liver, because its parenchymal cells, principally hepatocytes, play prime roles in drug metabolisms and detoxifications [1, 2]. Therefore, creation of a liver-chimeric rodent, a rodent whose hepatocytes in liver are humanized by being replaced with human (h) hepatocytes (*h*-hepatocytes), might greatly contribute to R&D studies of drug development. Conventionally, mice have been preferred to rats, because their genetic data are richer and gene technology is applicable more easily in the former.

Hepatocyte-humanized mice were created as a suitable animal model for studying infection and propagation of hepatitis viruses (HVs) by using severe combined immunodeficient (SCID) mice as hosts that carry albumin (Alb)-promoter/enhancer-driven urokinase-type plasminogen activator (uPA) gene [3, 4]. As expected hepatitis viruses B and C (HBV and HCV) infected their livers as the liver in human body when the mice were injected with sera from HBV/HCV patients, which in turn provided us a piece of evidence for actual humanization of the mouse liver. Since then the chimeric mice have been thought to be an ideal animal model

*Address correspondence to this author at the Phoenixbio Co. Ltd., 3-4-1-Kagamiyama, Higashi, Hiroshima, Japan; Tel: +81-82-431-0016; Fax: +81-82-431-0017; Email: katsutoshi.yoshizato@phoenixbio.co.jp

1875-6220/12 $58.00+.00

for investigating mechanism of infection of these viruses and their proliferation therein and also to be quite useful test animals for discovery and characterization of anti HCV/HBV drugs [5].

Usefulness of chimeric mice as experimental tool depends on the extent of replacement of host hepatocytes with transplanted *h*-hepatocytes, because the presence of residual mouse (m)-hepatocytes (*m*-hepatocytes) hinders researchers from determining correct phenotypes of *h*-hepatocytes and would even affect the functions and activities of *h*-hepatocytes. It is clear that generation of chimeric mice whose livers are composed of mostly *h*-hepatocytes is especially vital to testing for metabolism and detoxification of drugs. Mice completely replaced with *h*-hepatocytes would be ideal, which, however, have not been attainable yet up to now in a reproducible manner. The extent of *h*-hepatocyte replacement is practically estimated by measuring concentrations of human Alb (hAlb) in host blood using human-specific antibodies or, when necessary, is correctly determined immunohistochemically as the number ratio [replacement index (RI)] of *h*-hepatocytes to total *h*- and *m*-hepatocytes using hepatocyte-specific proteins such as cytokeratin (CK) 8/18 as antigens. Liver sections are stained with the corresponding human-specific antibodies. The ratio of immuno-positive to examined entire area represents RI. We first developed methods and technologies to reproducibly produce chimeric mice with RI >70% using homogeneous populations of *h*-hepatocytes derived from individual donors [6]. Utilizing such chimeric mice with high RIs we were able to demonstrate that chimeric livers showed expression profiles of genes and proteins of major members of cytochrome P450 (CYP) similar to those of hepatocyte donors in a drug-dependent manner, strongly supporting our expectation that chimeric mice could be utilized as a useful animal model for predicting human metabolic profiles of test drugs [6]. The original methodology of chimeric mouse production has further been improved to a level of mass-production of homogenous chimeric mice with RI = ~90%, which enabled us to industrialize chimeric mice for drug testing [7, 8].

"Ready for use"-type availability of reproducible high-RI chimeric mice accelerated their detailed characterization with respect to propagation of *h*-hepatocytes, hepatic architectures, profiles of CYPs against various drugs (Phase I pathways), conjugation pathways (Phase II), and transports of known drugs, and infection and proliferation of HCV/HBV [7, 8]. Repopulation processes of *h*-hepatocytes in the damaged host liver were also investigated focusing on epitheliomesenchymal interactions between *h*-parenchymal cells and mouse non-parenchymal cells [9]. Recently, we reported an endocrinological problem inherent to chimeric mouse liver: *h*-hepatocytes were found to be growth hormone (GH)-deficient because the cells are indifferent to mouse GH, which causes *h*-hepatocyte lipogenesis [10].

Since we started on a task to provide researchers for drug R&D and those studying HCV/HBV infection mechanisms with *h*-chimeric mice with high RIs, ~7 years have passed. Collectively, hitherto accumulated data have proved that the chimeric mouse is appreciably humanized in the metabolic profiles of known drugs and HCV/HBV infection mechanisms in spite of the fact that the nonparenchymal tissues of the liver are totally composed of mouse cells and extracellular matrices. Thus, interests in chimeric mouse are increasing as a test animal model for predicting metabolic profiles of general and anti HCV/HBV drugs in pharmaceutical areas. We have had opportunities to review *h*-chimeric mouse studies emphasizing the "similarity" of *h*-hepatocyte characteristics between human liver and *h*-chimeric mouse livers [7, 8]. The present article aims to review present status of chimeric mouse studies emphasizing the "dissimilarity" of *h*-hepatocytes between the two livers with respect of hepatic architechtures, *h*-hepatocyte growth capacity, hepatocyte-nonparenchymal cell interactions, and endocrinological features and lipid metabolisms.

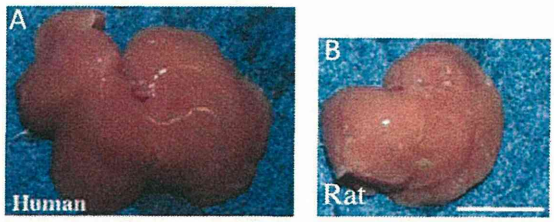

Fig. (1). Representative gross appearance of livers from *h*- and *r*-hepatocyte chimeric mice. *h*- and *r*-chimeric mice were generated by transplanting hepatocytes from a 9-year-old boy (**A**) and a 13-week-old male Fisher 344 rat (**B**). The *h*- and *r*-chimeric mice were killed 90 and 100 days post-transplantation, respectively their livers were photographed and analyzed for determining RIs and the ratios ($R_{L/B}$) of liver weight against body weight. The RI for the *h*- and *r*-chimeric mouse was 92 and 100%, respectively and $R_{L/B}$ 19.3 and 6.5%, respectively. Bar represents 1 cm. The photos are cited from the literature No. 9.

TISSUE ARCHITECTURES OF CHIMERIC MOUSE LIVER

The success in generating hepatocyte-humanized mice itself indicates that both donor hepatocytes and host nonparenchymal tissues could reconcile each other and manage well to reconstruct the chimeric liver. To measure the difficulty (easiness) of this reconciliation and management, we compared the chimerism by *h*- and rat (*r*) hepatocytes generated by transplanting *h*- and *r*-hepatocytes in uPA/SCID mice under the same conditions [9]. The obtained results clearly showed the much easiness in producing rat chimerism compared to human chimerism. First, repopulation speed of *h*-hepatocytes (~8% replacement/week) was much slower than that of *r*-hepatocytes (~30%/week). *h*-Hepatocytes require approximately four times longer time of periods to complete repopulation than *r*-hepatocytes. Second, *r*-hepatocyte repopulation was terminated with the complete repopulation (RI = 100%) at 3 weeks after transplantation, but that of *h*-hepatocytes was terminated with incomplete repopulation (~70% in average) even at 8 weeks posttransplantaion. Livers of *h*-hepatocyte and *r*-hepatocyte chimeric mice (RI = 94 and 100% for the former and latter, respectively) both looked macroscopically normal and healthy except that the former (Fig. **1A**) was quite bigger in volume than the latter (Fig. **1B**). Semi-macroscopic views of each of six among seven liver lobules are shown in (Fig. **2A**), which was obtained from a chimeric mouse that had been transplanted with 10^6 hepatocytes from a 6-year-old girl. The

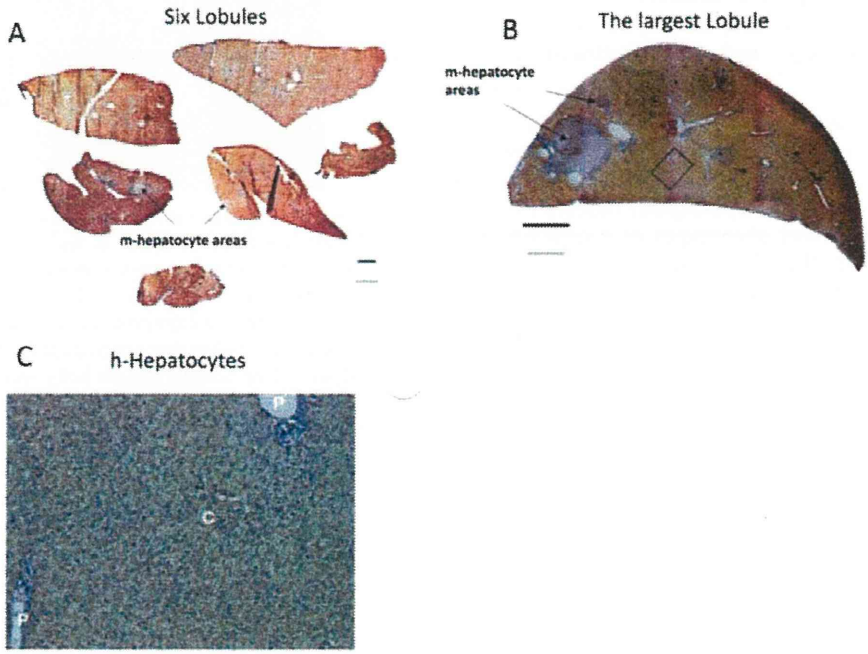

Fig. (2). Semi-macroscopic views of *h*-chimeric mouse lobules. *h*-Chimeric mice were produced with hepatocytes from a 6-year-old girl (**A**) and a 9-month-old boy (**B**). The rectangular area indicated in B was enlarged in C. See detailed explanations of the photos in the text. Bars in A, B, and C represent 1 μm, 1 μm and 100 mm, respectively. P and C in C indicate the location of portal and central veins, respectively. The photos are cited from the literature No. 8.

mouse in this case was sacrificed 77 days post-transplantation and its six liver lobules were sectioned for h-CK8/18 staining to locate *h*-hepatocyte regions. RI reached as high as ~99%. Quite small *m*-hepatocytic regions were present as indicated by arrows. A similar view of the largest lobule is shown in (Fig. **2B**) obtained from a chimeric mouse with RI = 82% that had been transplanted with 7.5 x 10^5 9-month-old boy's hepatocytes and killed at 80 days after transplantation. Its histology shows the well organized architectures of hepatic plates consisting of *h*-hepatocytes and *m*-nonparenchymal cells with the well-developed sinusoidal streams between portal and central veins (Fig. **2C**).

Hepatocytes are the parenchymal cells of the liver that pursuit "liver function". The hepatic nonparenchyma contains several species of cells such as sinusoidal endotherial cells, stellate cells and Kupffer cells. These cells aggregate and construct the liver with following number ratios, hepatocytes:Kupffer cells:stellate cells:endothelial cells = 52: 18: 8: 22 (%) in the case of mouse [11]. Hepatocytes are closely apposed in an orderly fashion and concentrate in a structurally stable mass called the hepatic plate by direct intercellular adhesions, which are structurally connected with nonparenchymal cells, forming liver-specific unique architectures including sinusoids where liver cells such as hepatocytes, stellate cells, Kupffer cells, and capillary cells communicate each other (Fig. **3**) [12]. The Kupffer cell and the pit cell (NK cell) rest on the fenestrated endothelial cell that contacts the poorly developed basement membrane of the sinusoid. A unique structure is formed between the hepatocyte plate and the sinusoidal basement membrane, which is defined as the space of Disse. The stellate cell, storing vitamin A in the lipid droplets, is located in this space, extending interhepato-

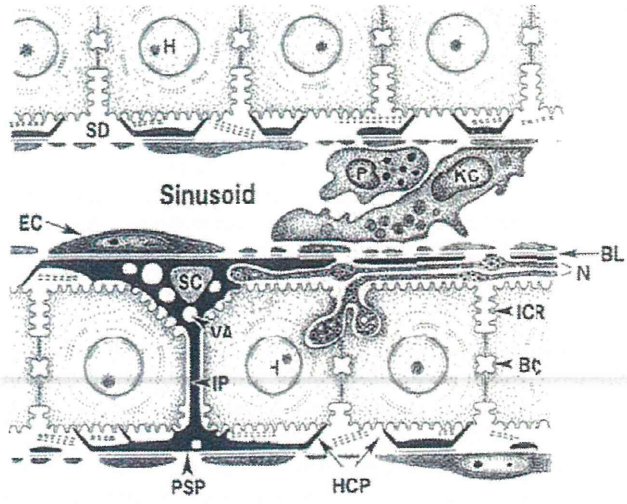

Fig. (3). Histological organization of mammalian liver tissue by hepatocytes and nonparenchymal liver cells. The tissue organization is schematically drawn focusing on the sinusoidal wall. The Kupffer cell (KC) and the pit cell (P) rest on the fenestrated endothelial cell (EC), which in turn contacts the hepatic stellate cell (SC) with poorly-developed basement membrane (BL) between both cells. The stellate cell, storing vitamin A in the lipid droplets (VA), extends interhepatocellular processes (IP) and perisinusoidal, or subendothelial processes (PSP), which encompass the endothelial tube. The stellate cells contact the hepatocyes (H) with their thorn-like microprojections or hepatocyte-contacting processes (HCP). The space between the endohelial cell-stellate cell complex and the hepatocyte is defined as the space of Disse (SD). Collagen fibrils and nerve fibers (N) course through the space of Disse. BC, bile canaliculus; ICR, interhepatocellular recess. This illustration is cited from the literature No. 12.

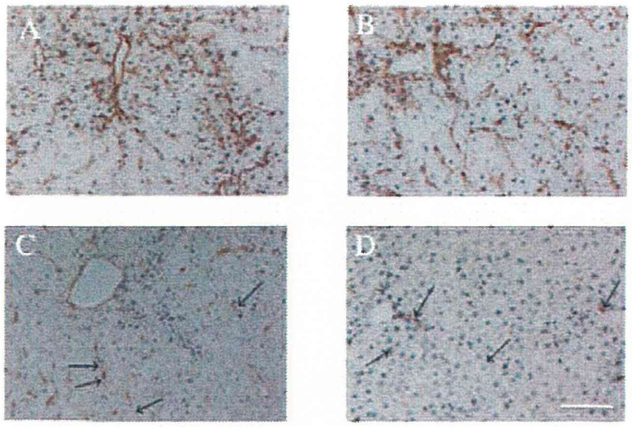

Fig. (4). Construction of chimeric liver by *h*-hepatocytes in association with *m*-nonparenchymal cells. uPA/SCID mice were transplanted with *h*-hepatocytes and allowed to grow until the repopulation of the liver was complete when the hosts were killed for examining histological features by immunohistological techniques. Sections were immunostained with antibodies for type IV collagen (**A**), laminin (**B**), stabillin (**C**), a marker of liver endothelial cells (a gift from Dr. A. Miyajima, Tokyo University), and BM8 (**D**), a marker of Kupffer cells. The immunosignals are brown. The arrows in (**C**) and (**D**) point to typical immunopositive cells. Bar represents 100 μm. These photos are cited from the literature No. 7.

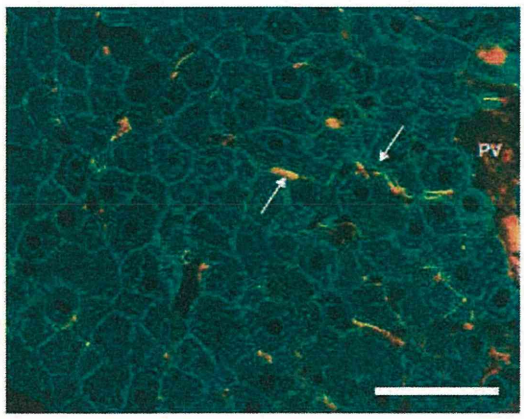

Fig. (5). Chimeric sinusoids formed by the elaborate collaboration of *h*-hepatocytes with *m*-nonparenchymal cells. A chimeric mouse was generated by transplanting 6-year-old girl's hepatocytes and killed 90 days posttransplantation when RI was ~80% for double-immunohistologically locating *h*-hepatocytes and *m*-hepatic stellate cells using antibodies against h-CK8/18 and desmin, respectively. *h*-Hepatocytes are stained green and *m*-stellate cells red. Arrows point to *m*-stellate cells. PV: portal vein. Bar represents 50 μm. This photo is sited from the literature No. 8.

cellular processes and perisinusoidal, or subendothelial processes, which encompass the endothelial tube. The stellate cells contact the hepatocyes with their thorn-like microprojections or hepatocyte-contacting processes. Collagen fibrils and nerve fibers course through the space of Disse.

Macro- and semi-macroscopical examinations shown in Figs. (**1** and **2**) suggest that *h*-hepatocytes normally communicate with *m*-nonparenchymal cells as *m*-hepatocytes do, which was supported by a study in which distributions of *h*-hepatocytes and *m*-stellate cells were examined by double-immunohistology on chimeric liver using animal species- and cell type-specific antibodies against CK8/18 for *h*-hepatocytes and desmin for *m*-stellate cells (Fig. **4**). *h*-Hepatocytes appear to be normally associated with *m*-stellate cells along the sinusoidal capillaries. Livers of *h*-chimeric mice with RI >70% were further examined to know normality/abnormality of the architectures constructed by *h*-hepatocytes, host nonparenchymal cells and host extracellular matrices (ECMs) using antibodies against type IV, laminin, stabilin for liver endothelial cells, BM8 for Kupffer cells, desmin for stellate cells, and human specific CK8/18 for hepatocytes. At glance these staining patterns first show a close association of *h*-hepatocytes with host nonparenchymal cells and second an apparent normal development of vascular systems with hepatic sinusoids (Fig. **5**).

The liver enlargement was only a macroscopic abnormality we noticed. To examine this phenomenon at the microscopical level, we made a detailed histological survey on sinusoidal architectures comparing to those of *r*-hepatocyte chimeric liver [9], because firstly rats are phyrogenetically quite close to mice and secondly it was shown that *r*-hepatocytes completely repopulate the liver of uPA/SCID mouse without any visible abnormal symptons [13]. Particularly we paid attention to the structures of hepatic plates and sinusoids, because they reflects the proliferation status of hepatocytes, *i.e.*, the hepatic plates are of single-cell layer and sinusoidal structures are compressed when hepatocytes are in non-proliferative (resting) conditions [14], but the former become multicell-layer thick and the latter become vague during vigorous hepatocyte proliferation [15]. *r*- and *h*-Hepatocyte chimeric mice were generated by transplanting hepatocytes from 13-week-old male Fisher 344 rats and a 9-month-old-male donor, respectively. They were sacrificed in the proliferation phase (P-phase) and the proliferation termination phase (T-phase). In the case of *r*-hepatocyte (*r*-hep) chimeric mice, the mice were killed at 2 weeks post-transplantation when the *r*-hepatocytes were in P-phase and RI was ~55%, and at 5 weeks when they were in T-phase and RI was100%. In the case of *h*-hepatocyte chimeric mice, the mice were killed at 5 weeks post-transplantation when the *h*-hepatocytes were in P-phase and RI was ~30%, and at 14 weeks when they were in T-phase and RI was ~70%. Their livers were subjected to investigating distributions of type IV collagen for sinusoidal spaces, multidrug resistance-associated protein (MRP2) for canalicular organic anion transporters (Fig. **6** and **7**). Normal livers from both human and rat specimens show the single-cell structures of hepatic plates on hematoxylin and eosin (H&E) sections (Fig. **6A** and Fig. **7A**, respectively). As we expected, both *h*- and *r*-hepatocyte chimeric livers at P-phase do not show such single-cell plates, but show multicell-layer-thick hepatic plates (Fig. **7D** for rat liver and data not shown for human liver). The MRP2 protein is randomly distributed in the intercellular space in P-phase (Fig. **7E** for rat liver and data not shown for human liver), sinusoidal structures are also not in an orderly fashion, losing vessel continuity along the portal-central axis. *r*-Hepatocyte chimeric livers regain the normal arrangement of hepatic plates and sinusoids, reconstructing the resting liver structure with single hepatic plates along the portal-central axis at 5 weeks after transplantation (T-phase)

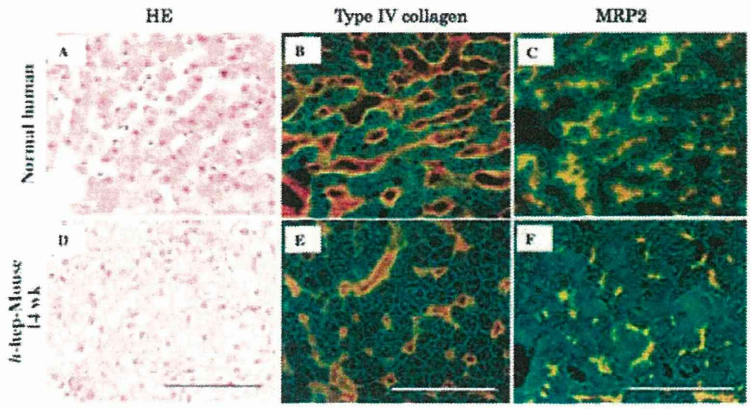

Fig. (6). Histological characteristics of *h*-hepatocyte chimeric mouse livers. Normal human livers were obtained from a 65-year-old female donor (**A-C**). *h*-Chimeric mice were generated by transplanting the hepatocytes from a 9-month-old male. The animals were sacrificed at 14 weeks (T-phase, **D–F**). Liver sections were stained with H&E (**A** and **D**) and for type IV collagen (red, **B** and **E**) and MRP2 (red, **C** and **F**). The sections of B, C, E, and F were additionally stained hCK8/18 (green) to identify transplanted *h*-hepatocytes. Scale bars shown in D, E, and F represent 100 μm. These Photos are cited from the literature No. 9.

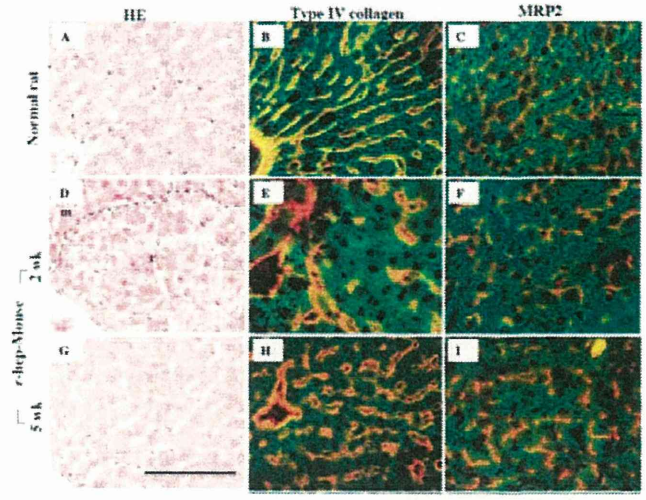

Fig. (7). Histological characteristics of *r*-hepatocyte chimeric mouse livers. Normal rat livers were obtained from 13-week-old male Fischer 344 rats (**A–C**). *r*-Hepatocyte chimeric mice were produced with 13-week-old male Fischer 344 rats and were sacrificed at two (P-phase, D–F) and five weeks (wks) after transplantation (T-phase, G–I). Liver sections were stained with H&E (**A**, **D**, **G**) and for type IV collagen (red, B, E, H) and MRP2 (red, **C**, **F**, I). The sections of B, C, E, F, H, and I were additionally stained for rRT1A (green) to identify transplanted *r*-hepatocytes. The dashed line in D shows the boundary between *r*-hepatocyte (r) and *m*-hepatocyte regions (m). Scale bar is shown in G and represents 100 μm. These Photos are cited from the literature No. 9.

(Fig. **7 G-I**). Quite differently, *h*-hep chimeric livers do not show single-cell hepatic plates, but show multicell-layer-thick plates and have obscure structures of sinusoids, structures characteristic of proliferative liver, even though they are in T-phase (14 weeks post-transplantation) (Fig. **6 D-F**). The MRP2 protein is also still randomly distributed in the intercellular space. These histological features indicate that *r*-hepatocytes are able to repopulate the mouse liver, by rapidly proliferating therein, reconstructing liver structures, and terminating replication when the normal resting structures are regained with single-cell hepatic plates and distinct structures of sinusoids that are arranged in an orderly manner along the portal-central axis. In contrast, *h*-hepatocytes appear to continue to proliferate even after they reconstruct structurally complete livers and RIs arrive at a plateaus, which is in a good agreement with the above-mentioned observation that *h*-chimeric, but not *r*-chimeric, livers are much enlarged compared with the original *m*-livers. This liver swelling was not a result of *h*-hepatocytic hypertrophy, but *h*-hepatocytic hyperplasia, because our morphometric examinations about the length of the long axis of hepatocytes on H&E sections showed that there are no significant differences among *m*-, *r*- and *h*-hepatocytes in chimeric mice. Observation of the enlarged *h*-chimeric livers led us to assume that crosstalks between parenchyma and nonparenchyma cells concerning termination of hepatocyte proliferation in the liver are not adequate in *h*-chimeric liver.

HYPERPLASIS OF CHIMERIC MOUSE LIVER

Liver is quite powerful in the regenerative ability [16]. When damaged, it somehow recognizes the presence of damaged cells and starts to increase DNA synthesis quite